CHARGED GEOSYNCHRONOUS DEBRIS PERTURBATION USING RAPID ELECTROMAGNETIC FORCE AND TORQUE EVALUATION

Joseph Hughes
Hanspeter Schaub
Department of Aerospace Engineering Sciences, University of Colorado, 431 UCB, Colorado Center for Astrodynamics Research, Boulder, CO 80309-0431

Space objects experience small perturbation torques and forces from their interaction with the local space environment. In the Geosynchronous orbit regime, objects have been shown to charge to 10s of kiloVolts in Earth's shadow, but also to kiloVolt levels in sun-lit conditions if the object's surface is not continuously conducting. This charging results in electrostatic torques and forces being produced due to the interactions with the local electric and magnetic fields. This paper investigates faster-than-realtime numerical methods such as Appropriate Fidelity Measures and the Multi-Sphere Method to approximate these forces and torques on uncontrolled High Area-to-Mass Ratio (HAMR) space debris. Numerical simulations show how these electrostatic forces and torques couple to stronger perturbations such as Solar Radiation Pressure to create position differences of hundreds of kilometers over periods of 12 hours, and thousands of kilometers over 48 hours for certain highly charged HAMR objects.

INTRODUCTION

Space situational awareness requires high-fidelity models to predict the positions of objects in orbit. High Area-to-Mass Ratio (HAMR) objects are especially sensitive to non-gravitational perturbations. This class of objects was first noticed by Schildknecht [1]. At Geosynchronous (GEO) altitudes, Solar Radiation Pressure (SRP) is a primary perturbation that shapes the orbit of light HAMR-like debris objects. SRP depends on the attitude of the object, which demands that attitude be taken into account when propagating these objects. Many of these HAMR objects are thought to be ripped pieces of Multi-Layer Insulation (MLI) [2]. Samples returned from the Hubble Space Telescope showed cracks in areas of constrained loading, and had a tendency to curl up when peeling off [3]. MLI may peel off of GEO sats, and could charge to very high potentials [4]. This charge will feel the Lorentz force ($\boldsymbol{F} = q\boldsymbol{v} \times \boldsymbol{B}$) which can affect the object's orbit or attitude in a small way. This small change can couple to stronger perturbations such as SRP to create large orbital changes.

Although SRP is the largest non-gravitational perturbation impacting HAMR debris objects, it may not be sufficient to explain all the observed HAMR object motions. The 28th International Symposium for Space Technologies and Sciences held in London, England, in June 2011 identified this issue. In particular, Professor Schildknecht discussed that families of HAMR objects have been identified whose mean motion changes remain very small, while the orbital angular momentum of these objects changes significantly with eccentricities varying up to 0.7. Natural charging of objects could result in a Lorentz force due to their interaction with the Earths magnetic field. The magnitude of such forces would depend on the relative velocity of the object with respect to the

magnetic field, as well as the absolute charge level. The Lorentz force, acting orthogonal to the orbital velocity, would be able to change the momentum without changing the orbit energy or mean motion. Wiesel recently reported in [5] some near-GEO debris objects which appear to accelerate *towards* the sun during the propagation interval. The cause of this motion is still being investigated, but charging is listed as a potential contributor. Früh et. al. where the first to publish results modeling the electrostatic charging effects on HAMR objects in [6]. This initial work includes Lorentz forces due to expected charging levels in a near-GEO orbit, along with lunar gravity, SRP and Eddy current effects on the orbit. As a result, the charged objects' orbit is shown to differ relative to the uncharged one by nearly a tenth of a degree in inclination and 0.002 in eccentricity after only 12 hours. However, electrostatic torques were not modeled in this earlier work, as the Mylar plates were modeled as effective point charges. Additionally, only the motion of a single shape with one set of initial conditions is studied.

This paper expands on this initial electrostatic perturbation study by employing novel electrostatic force models that allow for torque considerations to be included. In particular, this inclusion allows for the coupled translational and rotational impacts of charging to be considered. The recently developed Appropriate Fidelity Measures (AFMs) [7] are applied to the local flat electrostatic and magnetic environment force field conditions. This assumption of the ambient environment allows for a compact description of the electrostatic forces and torques on a general shape. Of interest is how the dynamics of a range of thin mylar sheets is impacted through the charge interaction with the environment. Two scenarios in particular are investigated. First, how much can the charging-induced Lorentz force by itself change an orbit. Second, when coupled with the SRP forces, how much can the inclusion of charging impact the orbital motion. Numerical simulations demonstrate the results where other disturbances such as lunar gravity and Eddy currents are included as well.

OVERVIEW MSM MODELS

Accurate models capable of providing analytic insight of torque and force are needed in many applications. For instance, electrostatic forces and torques have been considered as a means of touchless actuation for conducting satellites at GEO. [8, 9] The electrostatic force and torque can be computed using commercial high fidelity Finite Element Analysis (FEA) programs, or simpler FEA schemes such as the Method of Moments or Boundary Element Method. A recent addition is the Multi-Sphere Method, which uses hand-tuned parameters for the size and locations of spheres which are constrained to be equipotential [10, 11]. A subset of MSM is Surface MSM (SMSM) which places a large number of equal radius spheres uniformly across the surface of the body. The radius of all spheres is varied to achieve the known self capacitance. Although this method is slower to evaluate (due to the much larger number of spheres), it removes the need for hand tuning.

MSM emerged as a way to predict the force and torque with high-enough fidelity to be useful, while also evaluating fast enough to be practical. MSM approximates the satellite as a collection of spheres with variable position and radii. The voltage of any sphere is a function of both its' own charge and the charge on neighboring spheres. If these spheres are far enough away to be approximated as point charges, the voltage on the ith sphere is given by: [10, 11, 12]

$$V_i = \frac{1}{4\pi\epsilon_0}\frac{q_i}{R_i} + \sum_{j=1,\, j\neq i}^{N} \frac{1}{4\pi\epsilon_0}\frac{q_j}{r_{i,j}} \tag{1}$$

Where q_i and R_i are the charge and radius of the ith sphere, respectively, and $r_{i,j}$ is the distance between spheres i and j. If the voltages of each sphere are given by $\boldsymbol{V} = [V_1, V_2, ...V_N]^T$ and the

charges are given by $\boldsymbol{q} = [q_1, q_2, ...q_N]^T$, the relationship between the two is $\boldsymbol{V} = [C]^{-1}\boldsymbol{q}$. Where $[C]$ is the position dependent capacitance (PDC) matrix whose inverse is defined below:

$$[C]^{-1} = \frac{1}{4\pi\epsilon_0}\begin{bmatrix} 1/R_1 & 1/r_{1,2} & \cdots & 1/r_{1,N} \\ 1/r_{2,1} & 1/R_2 & \cdots & r_{2,N} \\ \vdots & \vdots & \ddots & \vdots \\ 1/r_{N,1} & 1/r_{N,2} & \cdots & 1/R_N \end{bmatrix} \tag{2}$$

Since the voltage is assumed known, and to be uniform across the spacecraft and the charges are needed to compute forces and torques, this matrix can be inverted and solved for the charge on each sphere. Once the charges are known the forces and torques can be computed as shown in Eqns. (3) and (4). We assume an origin at the center of mass of the body for $\boldsymbol{r}_i$ and allow $\boldsymbol{E}$ and $\boldsymbol{B}$ to vary within the body and indicate the velocity of each sphere with respect to the magnetic field as $\boldsymbol{v}_i$.

$$\boldsymbol{F} = \sum_{i=1}^{N} \big(\boldsymbol{E}(\boldsymbol{r}_i) + \boldsymbol{v}_i \times \boldsymbol{B}(\boldsymbol{r}_i)\big) q_i \tag{3}$$

$$\boldsymbol{L} = \sum_{i=1}^{N} \boldsymbol{r}_i \times \big(\boldsymbol{E}(\boldsymbol{r}_i) + \boldsymbol{v}_i \times \boldsymbol{B}(\boldsymbol{r}_i)\big) q_i \tag{4}$$

MSM is an accurate and fast way to solve for the forces and torque on a spacecraft. However, it relies on knowledge of the position and size of all spheres in the model which are obtained by fitting MSM parameters to a set of E-force truth data. This process can be optimized [13], especially if constraints are used.

The MSM parameter optimization can be simplified with the Surface MSM (SMSM) process at the expense of requiring a larger set of MSM spheres. SMSM places spheres of equal radii uniformly on the surface of the conductor. [14] The radii of all spheres is then varied until the MSM model has the same scalar self capacitance value as the physical object. The self capacitance is determined using a commercial FEA solver. This one-dimensional search results in MSM models with many more spheres (usually a few hundred rather than 2 or 3) that are slower to evaluate, but removes the need for the challenging MSM parameter optimization.

A example SMSM model for a template "box and panel" spacecraft near a sphere is shown in Fig. 1. The spheres are all the correct size, and the color indicates the charge. As one can see, the charge tends to concentrate at the corners of the conductor. SMSM can provide very accurate answers with only a one dimensional optimization. In this analysis SMSM models are used not for force, but rather to make static body-fixed parameters for Appropriate Fidelity Measures (AFM) models, which are discussed next.

AFM MODELS FOR LOCALLY FLAT FORCE FIELDS

Overview of General Formulation

Another recent addition to the methods for estimating electrostatic force and torque on a body is Appropriate Fidelity Measures (AFMs) which uses the first few terms in a binomial series to calculate moments of the charge distribution which can be used to estimate the force and torque. Formula for the force and torque on a conductor as functions of these measures in a flat and radial

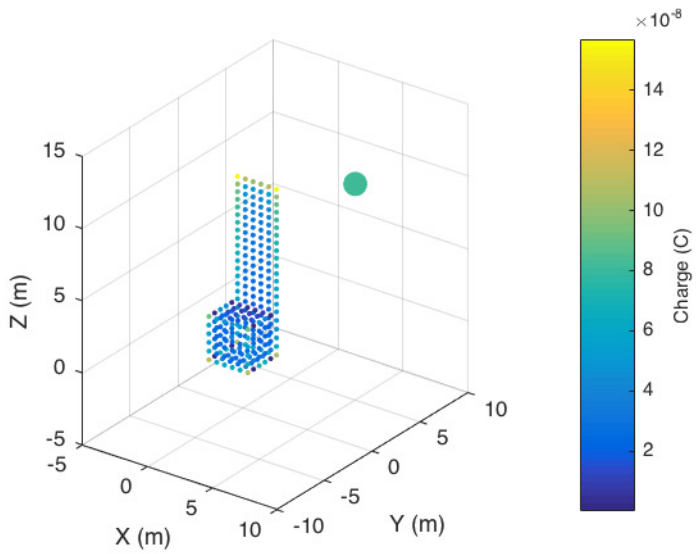

Figure 1. Example SMSM model for template spacecraft and sphere

field are shown in [7]. These measures can also be predicted from the voltage of each craft, and the ambient field.

In this analysis, only the force and torque due to a flat ambient field is needed. Although electric fields are observed in L shells similar to GEO [15], they are typically oscillatory and would not change an orbit, although they may be able to cause shape changes in flexible materials. The Lorentz field $\boldsymbol{v} \times \boldsymbol{B}$ is sustained and much stronger even though the velocity is small for a near-geostationary object. Although the strength and direction of the earth's magnetic field changes on a large scale, the change across a small body like a spacecraft is negligible. The differential force on a differential charge moving at $\boldsymbol{v}$ subject to $\boldsymbol{E}$ and $\boldsymbol{B}$ fields is given by [12]:

$$\mathrm{d}\boldsymbol{F} = \mathrm{d}q(\boldsymbol{E} + \boldsymbol{v} \times \boldsymbol{B}) \tag{5}$$

The torque about the center of mass on a body is defined as $\int_B \boldsymbol{r} \times \mathrm{d}\boldsymbol{F}$, where $\boldsymbol{r}$ points from the center of mass to the volume element. Using the differential force to find the force and torque on a body gives:

$$\boldsymbol{F} = \int_B (\boldsymbol{E} + \boldsymbol{v} \times \boldsymbol{B})\mathrm{d}q \tag{6}$$

$$\boldsymbol{L} = \int_B \boldsymbol{r} \times (\boldsymbol{E} + \boldsymbol{v} \times \boldsymbol{B})\mathrm{d}q \tag{7}$$

Locally Flat Force Field Approximation

To calculate the force experienced by a spacecraft in a flat field, the velocity variation over the body can be accounted for. The velocity is the orbital velocity $\boldsymbol{v_o}$ plus the transport velocity: $\boldsymbol{\omega}_{\mathcal{B}/\mathcal{E}} \times \boldsymbol{r}$, where $\boldsymbol{\omega}_{\mathcal{B}/\mathcal{E}}$ is the angular velocity between the satellite body frame $\mathcal{B}$ and the magnetic field

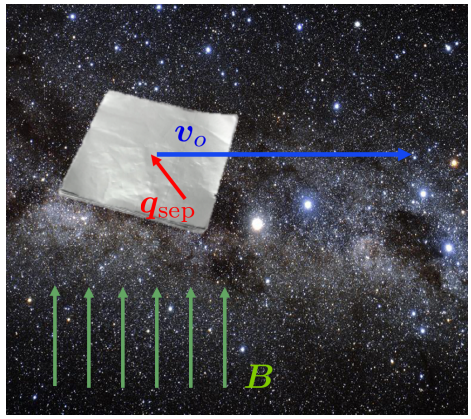

Figure 2. Flat External Field Configuration

frame $\mathcal{E}$. Letting $\boldsymbol{v} = \boldsymbol{v}_o + \boldsymbol{\omega}_{\mathcal{B}/\mathcal{E}} \times \boldsymbol{r}$ in Eq. (6):

$$\boldsymbol{F} = \boldsymbol{E} \int_B \mathrm{d}q + \int_B (\boldsymbol{v_o} + \boldsymbol{\omega}_{\mathcal{B}/\mathcal{E}} \times \boldsymbol{r}) \times \boldsymbol{B}\, \mathrm{d}q \tag{8}$$

$$= \boldsymbol{E} \int_B \mathrm{d}q - (\boldsymbol{B} \times \boldsymbol{v_o}) \int_B \mathrm{d}q - \left(\boldsymbol{B} \times \boldsymbol{\omega}_{\mathcal{B}/\mathcal{E}} \times \int_B \boldsymbol{r}\, \mathrm{d}q \right) \tag{9}$$

$$= \boldsymbol{E}\, Q - (\boldsymbol{B} \times \boldsymbol{v_o})\, Q - \boldsymbol{B} \times (\boldsymbol{\omega}_{\mathcal{B}/\mathcal{E}} \times \boldsymbol{q}_{\text{sep}}) \tag{10}$$

Where the total charge is Q, and the charge separation vector $\boldsymbol{q}_{\text{sep}}$ is defined as a generalization of the dipole moment [12].

$$Q = \int_B \mathrm{d}q \qquad \text{and} \qquad \boldsymbol{q}_{\text{sep}} = \int_B \boldsymbol{r} \mathrm{d}q \tag{11}$$

Next the assumption is made that the body rotation rates are small enough such that the orbital velocity $\boldsymbol{v}_o$, even taken in the ECEF frame, is much larger than the transport velocity $\boldsymbol{\omega}_{\mathcal{B}/\mathcal{E}} \times \boldsymbol{r}$. For a spacecraft with $r = 1$ m, $\omega_{\mathcal{B}/\mathcal{E}} = 1$ deg/sec, and an ECEF orbital velocity of 1 km/sec, the ratio of the transport velocity to the orbital velocity will be less than 10^{-5}. With this assumption the transport term is dropped leaving:

$$\boldsymbol{F} = (\boldsymbol{E} + \boldsymbol{v}_o \times \boldsymbol{B})\, Q \tag{12}$$

Substituting the transport velocity expression into Eq. (7) and simplifying, the electrostatic torque is found to be:

$$\boldsymbol{L} = -(\boldsymbol{E} + \boldsymbol{v_o} \times \boldsymbol{B}) \times \boldsymbol{q}_{\text{sep}} + \boldsymbol{\omega}_{\mathcal{B}/\mathcal{E}} \times \int_B (\boldsymbol{B} \cdot \boldsymbol{r}) \boldsymbol{r} \mathrm{d}q \tag{13}$$

$$\tag{14}$$

Much like a pendulum experiences a torque that aligns an offset mass with a gravity field, the first term describes a torque that aligns the dipole moment $\boldsymbol{q}_{\text{sep}}$ with $\boldsymbol{E} + \boldsymbol{v_o} \times \boldsymbol{B}$. The second term provides a torque perpendicular to both the rotation and the magnetic field, and quadratically proportional to the charge separation. This term is only significant when $\boldsymbol{v}_o$ is comparable to $r\boldsymbol{\omega}_{\mathcal{B}/\mathcal{E}}$, which

only happens at extremely fast spin rates for near-geostationary objects. If this term is neglected, the torque is given by:

$$\boldsymbol{L} = -(\boldsymbol{E} + \boldsymbol{v_o} \times \boldsymbol{B}) \times \boldsymbol{q}_{\text{sep}} \tag{15}$$

This torque compares to the torque on a dipole in a flat field found in [12] and [16]. Compared to the general series-based AFM solutions developed in [7], the first-order electrostatic force and torque expansions in Eqs. (12) and (15) are the exact solution if the above body spin rate assumptions are valid.

Note that both MSM and AFMs produce this algebraic form of the electrostatic force and torque of a general body in a flat field. Consider a generic MSM model with N spheres. The electric and magnetic fields do not change across the body in Eqns. (3) and (4) and are taken outside the sum. The total force is:

$$\boldsymbol{F} = \sum_i^N q_i(\boldsymbol{E} + \boldsymbol{v} \times \boldsymbol{B}) = (\boldsymbol{E} + \boldsymbol{v} \times \boldsymbol{B}) \sum_i^N q_i = (\boldsymbol{E} + \boldsymbol{v} \times \boldsymbol{B})Q \tag{16}$$

This is the same result as was found using AFMs.

To derive the MSM torque in a flat field, only half of the full field can be moved outside of the sum because the velocity with respect to the magnetic field will vary over the body if the body is spinning. Dividing the velocity of each sphere into its orbital and transport components as before gives:

$$\boldsymbol{L} = \sum_i^N \boldsymbol{r}_i \times (\boldsymbol{E} + (\boldsymbol{v}_o + \boldsymbol{\omega} \times \boldsymbol{r}_i) \times \boldsymbol{B})q_i \tag{17}$$

$$= \sum_i^N \boldsymbol{r}_i \times (\boldsymbol{E} + \boldsymbol{v}_o \times \boldsymbol{B})q_i + \sum_i^N \boldsymbol{r}_i \times \big((\boldsymbol{\omega} \times \boldsymbol{r}_i) \times \boldsymbol{B}\big)q_i \tag{18}$$

If the same assumption of the orbital velocity being much larger than the transport velocity is used, the second term drops out and the fields can be brought outside the sum:

$$\boldsymbol{L} = \sum_i^N \boldsymbol{r}_i \times (\boldsymbol{E} + \boldsymbol{v}_o \times \boldsymbol{B})q_i \tag{19}$$

$$= -(\boldsymbol{E} + \boldsymbol{v}_o \times \boldsymbol{B}) \times \sum_i^N \boldsymbol{r}_i q_i \tag{20}$$

Noticing the dipole $\boldsymbol{q}_{\text{sep}} = \int_b \boldsymbol{r}\mathrm{d}q = \sum_i^N \boldsymbol{r}_i q_i$ gives

$$\boldsymbol{L} = -(\boldsymbol{E} + \boldsymbol{v}_o \times \boldsymbol{B}) \times \boldsymbol{q}_{\text{sep}} \tag{21}$$

Once again, this result is equivalent in form to the AFM answer. This is only true because the differential force does not vary throughout the body, and no truncated binomial expansion is needed to approximate it.

Determining the AFM Parameters

The above formulas give the exact force and torque on a general body in a flat field if the body spin rate is sufficiently low, however, they assume knowledge of the total charge and the dipole. Both of these variables are a function of the specific body shape and change with time and the local space weather environment. Ways to predict the total charge Q and the dipole $\boldsymbol{q}_{\text{sep}}$ are outlined next.

If the voltage V is known, Q can easily be obtained through $Q = C_s V$ where C_s is the self capacitance, which can be found once using a commercial FEA tool. The voltage on a space craft is a function of the solar flux, plasma environment, and the material properties of the spacecraft. There are many tools for predicting this voltage including analytical current balance methods as shown in [17] or with computational tools such as NASCAP or SPIS.

Predicting the dipole is slightly more complex. The dipole can be thought of as the total charge Q multiplied by the separation of the center of charge from the center of mass. The charge will increase with the voltage, which will increase the magnitude of the dipole but not change the direction. An ambient field will push all the charge to one end of the spacecraft. How far an ambient field is able to move the center of charge is dependent on the geometry and attitude of the spacecraft with respect to the ambient field. These two effects are lumped into the following equation [7]:

$$\boldsymbol{q}_{\text{sep}} = \boldsymbol{\chi}_S V + [\chi_A]\boldsymbol{A} \tag{22}$$

Both of these susceptibilities ($\boldsymbol{\chi}_S$ and $[\chi_A]$) are found empirically by recording the charge distribution at different voltages and ambient fields using an FEA solver, or from a higher fidelity MSM model. In this analysis, a SMSM model with 100 spheres is used to generate the susceptibilities. If $[R]$ contains the positions of all MSM spheres from the center of mass, and $\boldsymbol{q}$ is a vector of the charges on each sphere the dipole can be formed as:

$$[R] = \begin{bmatrix} x_1 & \dots & x_N \\ y_1 & \dots & y_N \\ z_1 & \dots & z_N \end{bmatrix} \tag{23}$$

$$\boldsymbol{q}_{\text{sep}} = [R]\boldsymbol{q} \tag{24}$$

using the capacitance relation shown explicitly in Eqn. (2) to find the charges gives

$$\boldsymbol{q}_{\text{sep}} = [R]([C]\boldsymbol{V} + [C][R]^T\boldsymbol{A}) \tag{25}$$

$$\boldsymbol{q}_{\text{sep}} = \boldsymbol{\chi}_S V + [\chi_A]\boldsymbol{A} \tag{26}$$

where the new parameters $\boldsymbol{\chi}_S$ and $[\chi_A]$ are defined as:

$$\boldsymbol{\chi}_S = [R][C]\mathbb{1}(N, 1) \tag{27}$$

$$[\chi_A] = [R][C][R]^T \tag{28}$$

The force and torque on a charged conductor are therefore given by

$$\boldsymbol{F} = C_S V \boldsymbol{A} \tag{29}$$

$$\boldsymbol{L} = (\boldsymbol{\chi}_S V + [\chi_A]\boldsymbol{A}) \times \boldsymbol{A} \tag{30}$$

Note that $\boldsymbol{\chi}_S$ and $[\chi_A]$ are constants in the body frame much like the inertia tensor. Direction cosine matrices can be used to rotate $\boldsymbol{A}$ into the body frame or $\boldsymbol{\chi}_S$ and $[\chi_A]$ into whatever frame $\boldsymbol{A}$ is in to compute torque.

ORBIT MOTION IMPACT OF ONLY CONSIDERING CHARGING

Before numerical analysis, it is prudent to bound the effects that charging could have on an orbit. Consider a thin ($\frac{1}{4}$ mil) sheet of aluminized mylar one square meter in size. The self capacitance of this object will be near 40 pF, assuming a voltage of 30 kV gives a total charge of 1.2 μC. There is no sustained electric field at GEO, but the orbital velocity combines with earth's magnetic field to create a Lorentz force $\boldsymbol{F} = q\boldsymbol{v} \times \boldsymbol{B}$. Many uncontrolled GEO objects get pulled up to higher inclinations $\sim 16°$ by the moon's gravity [18]. This gives a velocity with respect to the magnetic field of $v = v_o \sin(i) = 3.075 \frac{\text{km}}{\text{s}} \sin(16°) \approx 1$ km/s. The B field at GEO is near 100 nT, which gives an effective $\boldsymbol{E}$ field of 100 μN/m. Combining this effective electric field with the charge gives an upper bound of qvB =(1.2 μC)(1 km/s)(100 nT) = $1.2 * 10^{-10}$ N for this object. The sheet only weighs 8.8 grams, but the acceleration due to charging still only causes an acceleration of $1.36 * 10^{-8}$ m/s^2. As a comparison, the earth's point mass gravity at GEO is approximated by 9.8 m/s^2 (1/6.6)^2 = 0.225 m/s^2.

The upper bound for SRP is given by $F = PA = 4.57 * 10^{-6} \times 1$ N and an acceleration of $5.177 * 10^{-4}$ m/s^2. SRP is clearly the stronger force by nearly 5 orders of magnitude. The change in the Keplarian orbital elements will now be investigated. The force from charging must act perpendicularly to both the relative velocity and the magnetic field. However, assuming it to be in the velocity direction allows for easy analysis. Using Gauss' variation of parameters to calculate the perturbative effect gives the change in semi-major axis (SMA) over one day of [19]

$$\frac{\mathrm{d}a}{\mathrm{d}t}\Delta t = \frac{2a_s}{n}(1 \text{ day}) \approx 32 \text{ meters} \tag{31}$$

Whereas the change in SMA over a day from SRP is 1,230 km. Thus, the impact of electrostatic forces on their own tend to be negligible in comparison to the impact of the SRP forces. However, because SRP forces are sensitive to the objects attitude, the next section investigates the impact of natural charging if both SRP and Lorentz perturbations are considered together.

NUMERICAL ANALYSIS OF CHARGED GEOSYNCHRONOUS ORBIT

Orbital Perturbations Considered

Many perturbations influence the orbits of HAMR objects at GEO. Each perturbation considered is detailed in Tab. 1 with either the exact equation or a short description.

Table 1. Forces and Torques acting on Space Debris

Perturbation	Force	Torque
Earth gravity	Spherical Harmonics up to 4th order	$\boldsymbol{L} = \frac{3\mu}{R_c^5}\boldsymbol{R}_c \times [I]\boldsymbol{R}_c$
Lunar gravity	point-mass gravity	0
Solar gravity	point-mass gravity	0
SRP	Absorptive, specular, and diffuse reflection	$\boldsymbol{L} = \boldsymbol{r}_{\text{sep}} \times \boldsymbol{F}_{\text{SRP}}$
Electrostatic	$\boldsymbol{F} = Q\boldsymbol{v} \times \boldsymbol{B}$	$\boldsymbol{L} = \boldsymbol{q}_{\text{sep}} \times (\boldsymbol{v} \times \boldsymbol{B})$
Eddy Currents	0	$\boldsymbol{L} = ([M](\boldsymbol{\omega} \times \boldsymbol{B})) \times \boldsymbol{B}$

As with Früh et. al [6], the eddy current torque is included as well. When a conductor spins in a magnetic field, the mobile electrons move in loops because of induction. No net force is felt

because the current path is closed, but an eddy current torque is felt. Gomez recently developed a general method for calculating this torque [20] through

$$\boldsymbol{L} = ([M](\boldsymbol{\omega} \times \boldsymbol{B})) \times \boldsymbol{B} \tag{32}$$

where $[M]$ is the magnetic tensor. For a flat plate, the matrix $[M]$ is given by

$$[M] = C_T \frac{\sigma e}{4} \boldsymbol{n}\boldsymbol{n}^T \tag{33}$$

where σ is the conductivity, C_T is a constant dependent on shape and size, and $\boldsymbol{n}$ is a unit vector normal to the plane. For a rectangle with length l greater than width w, C_T is found using St. Venant beam theory:

$$C_T \approx \frac{lw^3}{3(1 + 1.38(\frac{w^2}{l^2})^{1.36})} \tag{34}$$

in the cases considered, the normal axis of the plate is $\hat{\boldsymbol{z}}$ which makes the torque equal to

$$\boldsymbol{L} = ([M](\boldsymbol{\omega} \times \boldsymbol{B})) \times \boldsymbol{B} = C_T \frac{\sigma e}{4} (\omega_1 B_2 - \omega_2 B_1) \begin{bmatrix} B_2 \\ B_1 \\ 0 \end{bmatrix} \tag{35}$$

It is interesting to note that if the plate is spinning about its axis of maximum inertia, ω_3 will be large and ω_1 and ω_2 will be small or zero. The eddy torque will also be small, and the object's spin will be relatively unaffected. If the object is tumbling, only the spin rates about the body 1 and 2 axes are removed and it will eventually fall into a stable spin about its axis of major inertia.

The magnitude of the SRP force is determined by the solar flux and the illuminated area. The direction is governed by the amount of light that is absorbed and reflected specularly and diffusely. The SRP force is given by [21]:

$$\boldsymbol{F} = p_{SRP} A \cos(\theta) \left[\rho_A \hat{\boldsymbol{s}} + 2\rho_s \cos(\theta) \hat{\boldsymbol{n}} + \rho_d (\hat{\boldsymbol{s}} + \frac{2}{3} \hat{\boldsymbol{n}} \right] \tag{36}$$

Where θ is the angle between the sun-pointing line and the face normal, $\hat{\boldsymbol{s}}$ is the sun-pointing vector, $\hat{\boldsymbol{n}}$ is normal to the plane, and $\rho_A, \rho_S,$ and ρ_D are the absorptive, specular, and diffuse coefficients, respectively, which must sum to unity.

The electrostatic perturbations depend on three constants $C_s, \boldsymbol{\chi}_S$ and $[\chi_A]$, which are used to translate the voltage and ambient field to the charge and dipole. These parameters are found as functions of plate size next.

Self Capacitance Estimation

Calculating the self capacitance of a square plate is a well-studied problem. J.C. Maxwell himself estimated it to be 0.40 pF for a 1 cm square [22], and current computation methods now estimate it at 0.4019 pF [23]. The self capacitance of two geometrically similar objects, will scale linearly with any dimension. For instance, the self capacitance of a sphere is given by $C = 4\pi\epsilon_0 R$. For a flat plate, capacitance can be expressed as $c = C/B$ where C is the true capacitance in Farads, and B is the bigger side of the plate. For a square plate B is just the edge length.

Reitan and Higgins [24] produced a very useful curve from which c can be extrapolated from the aspect ratio of the big to small side B/S. Ten points are read off this curve, and a power law is used to fit it with good accuracy ($r^2 = 0.9995$). The power law is shown below.

$$c = \left(0.402 * 10^{-10} \frac{\mathrm{F}}{\mathrm{m}}\right)\left(\frac{B}{S}\right)^{-0.4733} \tag{37}$$

The capacitance is used to convert the voltage, which can often be estimated from space weather parameters and is assumed to not depend on size or shape, to the charge. The amount of charge will dictate the magnitude of the force.

The capacitance grows linearly with size, the area grows quadratically, and the mass grows cubicly. This means that the acceleration due to an area-based perturbation such as SRP will go like $1/r$ while the acceleration from charging-based perturbations will go like $1/r^2$. This means charging will be most significant for small objects. Small objects are also the hardest to track from earth, but may still pose collision risks to GEO satellites, and have the largest departures from simple two body orbits.

AFM parameter estimation through SMSM

Once the self capacitance is known, the AFM parameters $\boldsymbol{\chi}_S$ and $[\chi_A]$ are estimated. There are many ways to estimate these parameters, the method used in this analysis is to generate a SMSM mesh for the chosen shape and compute the AFM parameters from the positions and sizes of the spheres as is shown in Eq. (27) and (28). The SMSM model is created by dividing the plate into N small squares of side length $\Delta x = \sqrt{BS/N}$ and placing a sphere at each node in the mesh. This sets three of the four free parameters associated with each sphere. The radii of all spheres is varied until the self capacitance of the MSM model is equivalent to the self capacitance of the plate computed from the empirical power law. Then each sphere is shifted by $\boldsymbol{r}_{\text{sep}}$ to account for the center of mass to center of area difference. Finally, Eq. (27) and (28) are used to compute $\boldsymbol{\chi}_S$ and $[\chi_A]$.

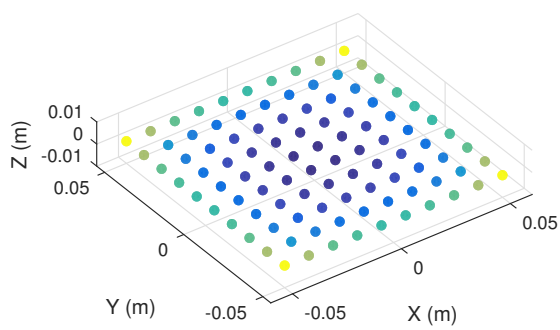

Figure 3. Flat plate modeled with SMSM, color indicates charge

The completed MSM model with correctly sized spheres and color indicating the charge on each sphere when charged to 30 kV is shown in Fig. 3. As one can see, more charge (shown as color) accumulates near the corners of the plate. The center of charge is located in the center of area,

but the center of mass, about which torques are taken, is removed by 2 mm in both $\hat{\boldsymbol{x}}$ and $\hat{\boldsymbol{y}}$. The center of charge will also move due to the Lorentz field, although this effect is small compared to the center of mass offset of 2.82 mm. For example, this 10 cm plate charged to 30 kV in a Lorentz field created from a velocity of 1 km/s orthogonal to a 100 nT magnetic field will only see a charge-center movement of 7.7 pm. The torque produced by the center of mass offset is a much stronger (more than 8 orders of magnitude) than the torque created by the induced effect. Nonetheless, both effects are included.

Since $\boldsymbol{\chi}_S$ is the dominant term, it is prudent to note that it can also be computed as $\boldsymbol{\chi}_S = C\boldsymbol{r}_{\text{sep}}$ where C is the capacitance in Farads and $\boldsymbol{r}_{\text{sep}}$ is a vector that points from the center of mass to the center of charge. This can be combined with Eq. (37) to yield the dominant electrostatic terms for a rigid plate.

Magnetic Field and Charging Models

Earth's magnetic field can be approximated as an inclined dipole for simple calculations close to earth. For more accurate calculations the IGRF model can be used, which takes many factors affecting earth's geodynamo into account. Outside Earth's magnetosphere, the magnetic field is purely a function of space weather and has little to no dependance on earth's own magnetic field. At GEO, these two effects combine to make a complex function of time and space weather parameters. The current state of the art for modeling this field is the Tsyganenko model [25]. There have been many versions and updates to this model, but in this analysis the 2001 version is used with GEOPACK 2008* for coordinate transforms.

This model has been implemented and is run at each time step. The time is assumed to be January 1, 2002, midnight, for all runs. The space weather parameters used are shown in Tab. 2 are representative, and are the same as is used by the Community Coordinated Modeling Center (CCMC) on their single-run website†

Table 2. Space weather parameters used for Tsyganenko model

Parameter	Value
Solar Wind Dynamic Pressure	4 nPa
Solar Wind Velocity	400 km/s
IMF B_y	6 nT
IMF B_z	-5 nT
DST	-30 nT

This produces a magnetic field that is deformed by the solar wind. As shown in Fig. 4, the field does not look like a tilted dipole and is deformed by the solar wind. Space weather will have a dramatic effect on the charging and the magnetic field strength and direction. Solar storms can cause high charge levels and cause strong electric and magnetic fields [15]. Since these fields are short-lived and oscillatory, the subsequent electrostatic perturbations are not directly capable of causing dramatic orbital changes. However, they may cause shape changes which may then change the orbit. For instance, consider a flexible sheet of conducting mylar, which when uncharged is

*http://ccmc.gsfc.nasa.gov/modelweb/magnetos/tsygan.html
†http://ccmc.gsfc.nasa.gov/requests/instant/tsyganenko.php

wadded into a small ball. If it suddenly charges from +10 V to -10 kV due to a solar storm, it may inflate and change its' area by a factor of 10 or 100. This would dramatically affect the SRP force and torque which would dramatically affect the orbit.

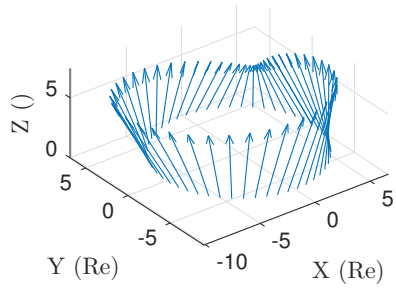

Figure 4. ECI Magnetic field used in this study, Z axis is arbitrary

The voltage of a conducting sheet is perhaps one of the easier spacecraft charging problems one could pose, nonetheless it is a still a hard problem. The voltage was modeled under very harsh charging conditions by Früh et. al. in [6] for a sheet with one side conducting and one of different dielectrics such as Kapton and Mylar. The most extreme voltage found was slightly more negative than -30 kV and occurred when using the very high ATS-6 flux. In this analysis, a simple and constant value of -30 kV is used to give a rough maximum for the charge level. In many circumstances, the voltage would be much smaller.

Numerical Propagation of Nominal Case Study

A nominal case of a thin rigid square of MLI is considered first. The material parameters are shown in Tab. 3. Any matrix values not explicitly defined are zero. The inertia tensor is computed assuming constant density.

Two simulations are run on the rigid plate, one including charging effects (electrostatic and eddy currents) and one without. This is done to investigate the magnitude of the charging induced perturbations. The Lorentz field by itself can only change the SMA by a few tens of meters per orbit, but electrostatic force and torque may couple to stronger perturbative forces which are sensitive to the orientation to create large position differences after only a few orbits.

In this nominal case, the final positions of the plate after 48 hours of propagation with and without charging effects differ by 1474 km. When compared with the nominal SMA of 42,164 km, this difference appears small, however it corresponds to 2 degrees if projected in the velocity-normal plane. Also, over a longer integration period such as a week this difference could be much larger. This difference is thought to be primarily due to electrostatic torque which re-orients the plate and changes SRP. If the object were spinning faster, eddy current torques would contribute more since they are proportional to the angular velocity.

While it is interesting to look at the departure of the classical orbital elements, it is perhaps more applicable to look at collision risk. Uncontrolled debris, especially HAMR debris can drift far away from their nominal geostationary orbit and may impact other spacecraft. The debris analyzed are inclined, so do not spend much time in the geostationary ring, but when they do pass through they have very high ($\sim$ 1 km/s) closing velocity.

The longitude and altitude departure from initial of both the charged and uncharged plate is shown

Table 3. Nominal HAMR propagation values [6, 26]

Parameter	Value
thickness	1/4 mil (6.35 μm)
density	1.39 g/cm^3
L_x	10 cm
L_y	10 cm
C	4.02 pF
$\boldsymbol{r}_{\text{sep}}$	$[2, 2, 0]^T$ mm
$\boldsymbol{\chi}_S$	$8.043 * [1, 1, 0]^T$ fF m
$\psi_A(1, 1)$	$5.393 * 10^{-11}$ F m^2
$\psi_A(2, 1), \psi_A(1, 2)$	$1.711 * 10^{-14}$ F m^2
$\psi_A(2, 2)$	$1.613 * 10^{-12}$ F m^2
ρ_A	0.5
ρ_S	0.2
ρ_D	0.3
σ_C	3.5*10^7 S/m
$M_{3,3}$	333.12 Sm^4

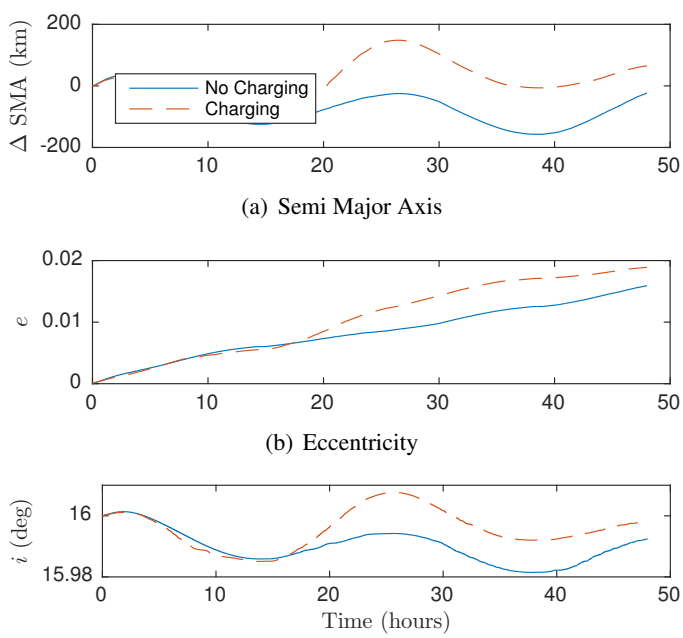

(a) Semi Major Axis

(b) Eccentricity

(c) Inclination

Figure 5. Change in classical orbital elements parameters due to charging

in Fig. 6 for the 48 hour integration time. As one can see, both plates drift by more than 6 degrees in longitude, and nearly 1600 km in altitude. Both craft pass through geosynchronous altitude three times and could impact operational spacecraft. This shows that propagating HAMR orbits at GEO is a very sensitive process, and electrostatic effects may need to be taken into consideration for some objects.

Additionally, if these plates originated from defunct spacecraft in GEO graveyard orbit, typically between 200 and 300 km above geosynchronous, they could easily pass back through GEO and pose a collision risk.

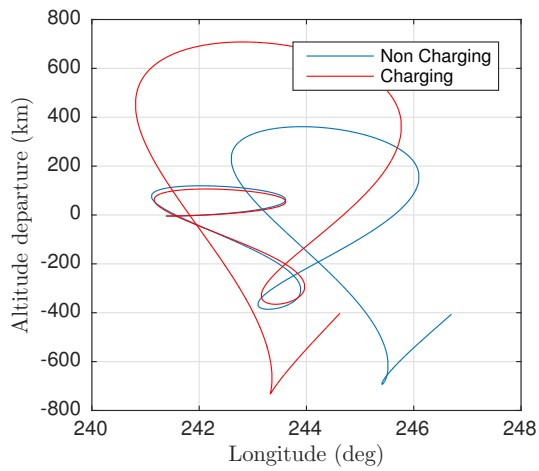

Figure 6. Longitude and altitude for plates with and without charging

As a comparison on the relative effect of charging related perturbations and initial conditions, this simulation was run again, but instead of keeping initial conditions the same and turning on charging, charging remained off for both runs but the initial attitude was changed from $\boldsymbol{\sigma} = [0, 0, 0]^T$ to $\boldsymbol{\sigma} = [0.1, 0, 0]^T$. This caused a final difference comparable to the distance caused by charging. This shows that propagation of HAMR objects is a very delicate and sensitive process, and electrostatic charging is one of the many things that need to be accounted for for very high fidelity propagation.

SPACE OBJECT SHAPE AND INITIAL STATES TRADE STUDIES

The single case of a 10 cm sheet showed significant differences caused by charging. To investigate the magnitude of charging effects on objects with different sizes and different initial conditions trade studies are performed. Running the two cases for 48 hours required 10 minutes of computer time, in the following trade studies a simulation time of 12 hours is used for faster analysis.

Plate Area and Aspect Ratio

The first trade undertaken is one between the aspect ratio, total area, and the scalar difference between the final positions of the plate propagated with charging effects and the plate propagated without.

The area A is varied logarithmically from 1 cm^2 to 1 m^2, and the aspect ratio α is varied linearly from 1 to 10. The big and small sides denoted B and S are then given by

$$B = \sqrt{A\alpha} \qquad S = B/\alpha \tag{38}$$

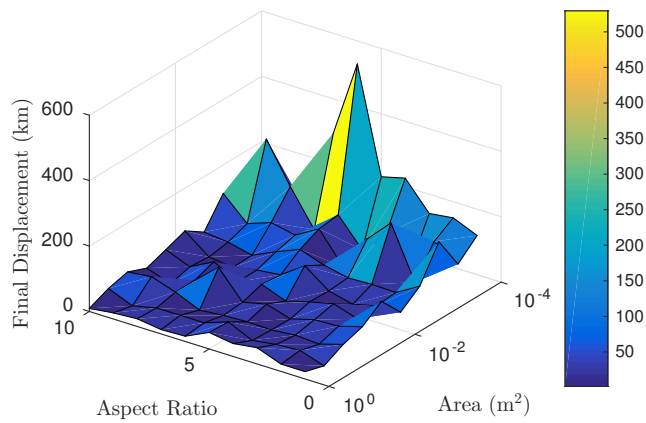

Figure 7. Differences in final state after 12 hours of propagating with and without charging effects

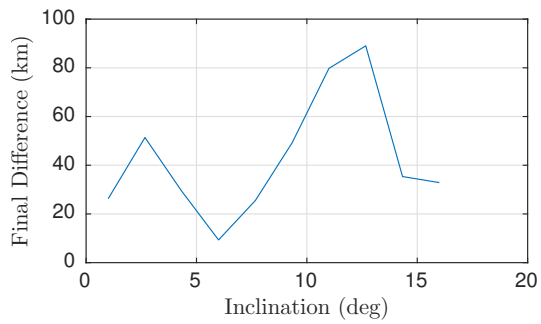

Figure 8. Influence of Initial Inclination on final difference

The offset between the center of mass and center of area is scaled to be 2% of corresponding side length:

$$\boldsymbol{r}_{\text{sep}} = [B/50, S/50, 0]^T \tag{39}$$

The results of this trade study are shown in Fig. 7. The differences caused by charging are more noticeable when the the object is small, with the maximum displacement being 529 km for this 12 hour integration time which corresponds to 0.72° if projected perpendicular to radial. Even for objects large enough to track (10 cm^2), differences over 100 km are not uncommon. Note that the Mylar plate have a very large surface to mass ratio. For larger, denser object such as a GEO satellite itself, the impact of charging will become negligible.

Initial Inclination

Electrostatic effects hinge on the velocity being non-zero and non-parallel to the magnetic field lines. The velocity with respect to the magnetic field is proportional to the sine of the inclination which means low inclination orbits should see less of an effect. A trade study in initial inclination is performed by varying the initial inclination from 1° to 16° linearly. The results are shown in Fig. 8.

There seems to be an upward trend with inclination, which would match intuition as electrostatic forces and torques increase with inclination. The trend is however hard to identify, and further study

perhaps including a Monte Carlo analysis randomizing initial orientations, is needed to establish a definite trend as the orientation changes couple into the orbit impact.

Initial attitude

The second trade study undertaken is in varying the initial attitude. An initially sun pointing plate will have maximum SRP force and torque which will help it spin up faster. An initial orientation orthogonal to the sun line will have virtually no SRP force or torque until a separate perturbation such as electrostatics or gravity gradients change the attitude.

The dimensionless variable α is used to measure just how much the spacecraft is initially sun pointing. If the unit vector pointing to the sun is $\hat{\boldsymbol{r}}_s$ and $\hat{\boldsymbol{k}}$ is a random vector perpendicular to $\hat{\boldsymbol{r}}_s$, the body z axis will align with

$$\hat{\boldsymbol{z}} = \alpha \hat{\boldsymbol{r}}_s + (1-\alpha)\hat{\boldsymbol{k}} \tag{40}$$

Setting $\alpha = 1$ will make the plate initially sun pointing. The body x axis is found to be a separate random unit vector perpendicular to $\hat{\boldsymbol{z}}$, and $\hat{\boldsymbol{y}}$ is found through $\hat{\boldsymbol{y}} = \hat{\boldsymbol{z}} \times \hat{\boldsymbol{x}}$. A direction cosine matrix is formed from this set, and from that an initial MRP attitude is found.

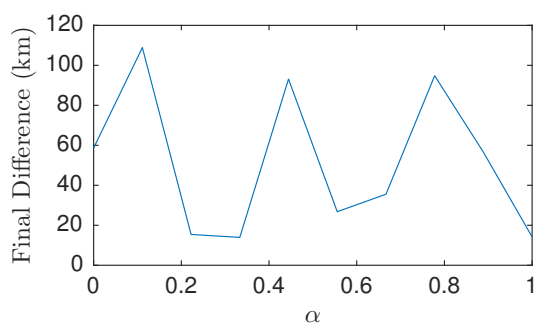

Figure 9. Difference in final positions as initial sun pointing angle changes

The difference in final positions with varying initial attitudes is shown in Fig. 9. These results illustrate the strong sensitivity to the initial orientation. Even relatively small changes can cause large orbit position departures after only 12 hours. This again demonstrates the importance of small perturbations such as electrostatics particularly for very lightweight objects if the propagation time is long.

Initial Spin Rate

Many uncontrolled objects are tumbling due to external perturbative torques. The fourth and final trade study is between the initial spin rate, which as been exactly zero in all previous simulations, and the distance between final states of the two simulations run with and without charging effects. The initial magnitude of the spin rate is varied logarithmically between 0.0001 °/sec and 5 °/sec, and is given about the axis $[0.2673, 0.5345, 0.8081]^T$ to create a general tumbling motion. The results are shown on a semi-log plot in Fig. 10. There is not an easily identifiable trend in initial angular rate either. However, the differences caused by changing the initial rate are large–nearly 100 km in some cases.

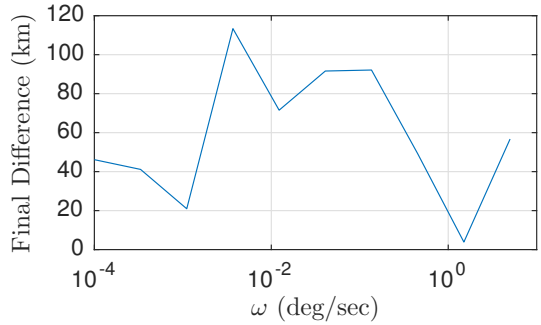

Figure 10. Difference in final positions as a function of initial spin rate

CONCLUSIONS

The problem of propagating a very lightweight HAMR object subject to multiple complex perturbations is a challenging one. The presented AFM and MSM models facilitate the faster-than-realtime numerical propagation of charged space objects in a magnetic field. Including or neglecting electromagnetic perturbations, such as electrostatic force and torque as well as eddy current torques, can cause 12-hour propagations of lightweight Mylar sheets to differ by at least a kilometer and sometimes more than 500 km. These HAMR objects are very sensitive and inclusion of small perturbations such as electrostatics may be necessary if the propagation time is long and the objects are known to charge. The differences in final position appear to be strong functions of size, aspect ratio, initial attitude, inclination, and initial rate, but the only trade study that shows a definite and easily-recognizable trend is size. Charging effects appear to be the most significant for small objects. This matches intuition as small objects will have the largest charging-related accelerations.

The charge levels used in this analysis are very large and the objects are extremely light and thin. This puts a possible upper bound on the effects of charging on an uncontrolled HAMR orbit. Future work is needed to consider the impacts of charging on heavier objects at less extreme voltages.

ACKNOWLEDGEMENT

This work was funded by research grant No. FA9550-15-1-0407 from the Air Force Office of Space Research.

REFERENCES

[1] T Schildknecht, R Muscia, M Plonera, G Beutlera, W Fluryb, J Kuuselac, J de Leon Cruzd, and L de Fatima Dominguez Palmerod. Optical observations of space debris in geo and in highly-eccentric orbits. *Advances in Space Research*, pages 901–911, 2004.

[2] T. Schildknecht, R. Musci, C. Frueh, and M. Ploner. Color photometry and light curve observations of space debris in geo. *Procedings of the Internaitonal Astronautical Congress*, 2008.

[3] Joyce A. Dever, Kirn K. de Groh, Jacqueline A. Townsend, and Jacqueline A. Townsend. *Mechanical Properties Degradation of Teflon FEP returned from the Hubble Space Telescope*. American Institute of Aeronautics and Astronautics, 1998.

[4] Joseph F. Fennell, H. C. Koons, MS Leung, and PF Mizera. A review of SCATHA satellite results: Charging and discharging. *1983.*, pages 3–11, 1983.

[5] William E. Wiesel. Estimating nongravitational accelerations on high area to mass ratio objects. *Journal of Guidance, Control, and Dynamics*, 0, Feb. 22 2015.

[6] Carolin Früh, Dale Ferguson, Chin Lin, and Moriba Jah. The effect of passive electrostatic charging on near-geosyncronous high area-to-mass ratio objets. *International Astronautical Congress*, 64, 2013.

[7] Joseph Hughes and Hanspeter Schaub. Appropriate fidelity electrostatic force evaluation considering a range of spacecraft separations. In *AAS/AIAA Spaceflight Mechanics Meeting*, Feb. 14–18 2016.

[8] Hanspeter Schaub and Daniel F. Moorer. Geosynchronous large debris reorbiter: Challenges and prospects. *The Journal of the Astronautical Sciences*, 59(1–2):161–176, 2014.

[9] Trevor Bennett, Daan Stevenson, Erik Hogan, Lauren McManus, and Hanspeter Schaub. Prospects and challenges of touchless debris despinning using electrostatics. *Advances in Space Research*, 56(3):557–568, 2015.

[10] Daan Stevenson and Hanspeter Schaub. Multi-sphere method for modeling electrostatic forces and torques. *Advances in Space Research*, 51(1):10–20, Jan. 2013.

[11] Daan Stevenson and Hanspeter Schaub. Multi sphere modeling for electrostatic forces on three-dimensional spacecraft shapes. In *AAS/AIAA Spaceflight Mechanics Meeting*, Charleston, South Carolina, Jan. 29 – Feb. 2 2012.

[12] David J. Griffiths. *Introduction to Electrodynamics*. Prentice Hall, 3rd edition, 1999.

[13] Philip Chow, Joseph Hughes, Trevor Bennett, and Hanspeter Schaub. Automated sphere geometry optimization for the volume multi-sphere method. In *AAS/AIAA Spaceflight Mechanics Meeting*, Feb. 14–18 2016.

[14] Daan Stevenson and Hanspeter Schaub. Optimization of sphere population for electrostatic multi sphere model. *IEEE Transactions on Plasma Science*, 2013.

[15] David M. Malaspina, John R. Wygant, Robert E. Ergun, Geoff D. Reeves, Ruth M. Skoug, and Brian A. Larsen. Electric field structures and waves at plasma boundaries in the inner magnetosphere. *Journal of Geophysical Research (Space Physics)*, 120:4246–4263, 2015.

[16] Douglas C. Giancoli. *Physics for Scientists and Engineers*. Pearson Prentice Hall, 2008.

[17] Shu T Lai. *Fundamentals of Spacecraft Charging: Spacecraft Interactions with Space Plasmas*. Princeton University Press, 2011.

[18] Paul V. Anderson and Hanspeter Schaub. Local orbital debris flux study in the geostationary ring. *Advances in Space Research*, 51(12):2195–2206, 2013.

[19] David A Vallado. *Fundamentals of Astrodynamics and Applications*. Microcosm Press, 4th edition, March 2013.

[20] N. Ortiz Gomez and S. J. I. Walker. Eddy currents applied to de-tumbling of space debris: feasibility analysis, design and optimization aspects. *Acta Astronautica*, 114:34–53, 2015.

[21] Bong Wie. *Space Vehicle Dynamics and Control*. AIAA Education Series, Reston, VA, 2nd edition, 2008.

[22] J.C. Maxwell. *A Treatise on Electricity and Magnetism*. Oxford University Press, 1893.

[23] D. N. De G. Allen and S. C. R. Dennis. The application of relaxiation methods to the solution of differential equations in three dimensions. *Quarterly Journal of Mechanics and Applied Mathematics*, 6:87, 1953.

[24] Daniel K. Reitan and Thomas J. Higgins. Accurate determination of the accurate determination of the capacitance of a thin rectangular plate. *Transactions of the American Institute of Electrical Engineers, Part I: Communication and Electronics*, 75(6):761–766, 1957.

[25] N. A. Tsyganenko. A magnetospheric magnetic field model with a warped tail current sheet. *Planetary and Space Science*, 37:5–20, 1989.

[26] Jay McMahon and Daniel J. Scheeres. A new navigation force model for solar radiation pressure. In *AIAA Journal of Guidance, Control and Dynamics*, volume 33, pages 1418–1428, 2010.